

Low-Noise Dual-Way Magnetron Power-Combining System Using an Asymmetric H-Plane Tee and Closed-Loop Phase Compensation

Xiaojie Chen^{ID}, *Graduate Student Member, IEEE*, Bo Yang^{ID}, *Student Member*, Naoki Shinohara^{ID}, *Senior Member, IEEE*, and Changjun Liu^{ID}, *Senior Member, IEEE*

Abstract—To meet the increasing power demands of microwave industries and scientific innovations, a dual-way magnetron (MGT) power-combining system based on an asymmetric H-plane tee combined with closed-loop phase compensation (CLPC) was developed and tested. Only one external injection was used, which could lock both frequencies of the two MGTs via the port coupling of the asymmetric H-plane tee. Additionally, phase control was achieved simultaneously in both MGTs. By tuning the external frequency, the frequencies of both MGTs could be shifted to optimize the power-combining efficiency. The optimal combining efficiency was 95.7%. By adjusting the phase of the external injection, the phase for the combining output was adjusted with a control scope in the 0°–360° range. The phase noise level of the combined output was largely inhibited by implementing only one closed-loop phase compensation subsystem. The phase jitter was limited to approximately $\pm 0.5^\circ$, and spur suppression ratios of -61.0 dBc/Hz at 10 Hz, -80.9 dBc/Hz at 100 Hz, -91.6 dBc/Hz at 1 kHz, and so on were achieved. Moreover, we deduced the corresponding power-combining theories in the asymmetric H-plane tee and noise reduction using the closed-loop compensation method. The numerical predictions qualitatively agreed with the experimental results. Additionally, this research reveals that the proposed techniques have great potential for future power-combining systems because they provide higher power output and noise reduction.

Index Terms—Closed-loop system, injection locking, magnetron (MGT), phase control, microwave power combining, phase noise.

I. INTRODUCTION

MAGNETRONS (MGTs) have attracted the attention of researchers for decades because of their remarkable

Manuscript received December 29, 2020; accepted January 6, 2021. Date of publication February 19, 2021; date of current version April 2, 2021. This work was supported in part by the National Natural Science Foundation of China under Grant 62071316, the Sichuan Science and Technology Program under Grant 2021YFH0152, and the China Scholarship Council under Grant 201906240240. (Corresponding authors: Naoki Shinohara; Changjun Liu.)

Xiaojie Chen is with the School of Electronics and Information Engineering, Sichuan University, Chengdu 610064, China, and also with the Research Institute for Sustainable Humanosphere, Kyoto University, Uji 611-0011, Japan (e-mail: xjchen9112@163.com).

Bo Yang and Naoki Shinohara are with the Research Institute for Sustainable Humanosphere, Kyoto University, Uji 611-0011, Japan (e-mail: yang_bo@rish.kyoto-u.ac.jp; shino@rish.kyoto-u.ac.jp).

Changjun Liu is with the School of Electronics and Information Engineering, Sichuan University, Chengdu 610064, China (e-mail: cjliu@ieee.org).

Color versions of one or more figures in this article are available at <https://doi.org/10.1109/TMTT.2021.3056550>.

Digital Object Identifier 10.1109/TMTT.2021.3056550

advantages such as low weight, low cost, high-efficiency dc-to-radio frequency (RF) conversion, and high-power microwave output. In applications using advanced materials, such as the synthesis of diamond films [1], microwave sintering of powdered metals [2], and other innovations that rely on promising high-power microwaves, continuous-wave (CW) MGTs are irreplaceable because they enable energy conservation and emission reduction. Brown *et al.* [3] proposed that CW MGTs are potential candidates as high-power microwave sources in microwave wireless power transmission (WPT) systems and space solar power stations. Shinohara *et al.* [4] used MGTs for practical WPT applications by developing phased arrays based on phase-controlled MGTs. Overett *et al.* [5] proposed that the MGTs are attractive, simple, and inexpensive RF systems for future accelerators. Dexter *et al.* [6] and Kazakevich *et al.* [7] demonstrated that a superconducting cavity can be driven by an injection-locked MGT transmitter with a phase jitter of less than or equal to $\pm 1^\circ$.

An MGT's output power is limited by the cavity's physical dimensions. The power-combining technique is an effective and commonly used method for combining multipath energy flows and gaining multifold output power with high combining efficiency. However, the operating frequency and phase of a free-running MGT fluctuate instantaneously. High-efficiency power combining cannot be achieved when the incoming signals are incoherent and uncontrollable. The injection-locking technique is an attractive method for improving the output quality and synchronizing the operating frequencies of different MGTs.

When the frequencies of MGTs are coherent, they are ready for high-efficiency power combining. For particle accelerator applications, Treado *et al.* [8] developed a dual-way injection-locked pulsed-MGT power-combining system with a power-combining efficiency of 92%. For industrial microwave use, Zhang *et al.* [9] realized a power-combining system via quasi-locking, which locked 2.45-GHz 1-kW MGTs with a combining efficiency of above 92%. Liu *et al.* [10]–[12] successfully developed the largest 2.45-GHz CW MGT system for dual- and four-way power combining with combining efficiencies constantly maintained over 90%. Park *et al.* [13] achieved an efficiency of approximately 93% for a dual-way MGT power-combining system with sideband noise suppression. Lai *et al.* [14] implemented the frequency-searching

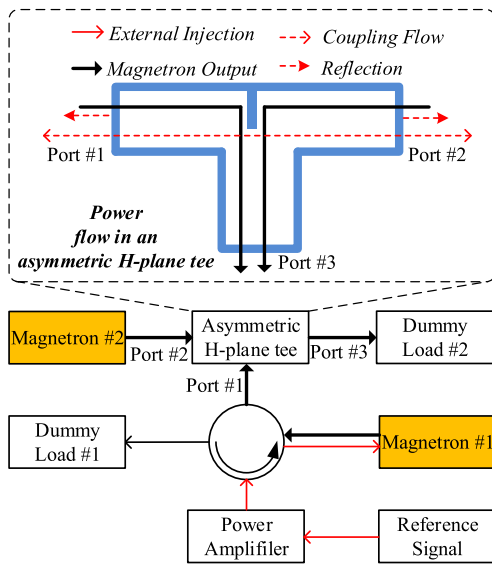


Fig. 1. Simplified schematic of the proposed dual-way magnetron combining system.

technique to achieve a phase-shifterless dual-way injection-locked power-combining system with a combining efficiency of above 94%. For WPT applications and to achieve beam forming (spatial power combining), Chen *et al.* [15] developed a 3.5-kW 2.45-GHz microwave transmission system based on four master–slave phase-controlled MGTs. Yang *et al.* [16] developed an active phased array using four 5.8-GHz MGTs with an output power of 1.3 kW; beam scanning was first achieved by the independent amplitude and phase control of each MGT.

To guarantee high combining efficiency in an N -way system, conventionally, N MGTs should be locked by implementing N injection subsystems, and at least $N - 1$ MGT phases should be simultaneously adjusted [8]–[16]. Nevertheless, the phase of the combining output cannot be adjusted or maintained constant except when all the MGTs' phases are controllable in real time [16]. The near-carrier noises of the output of a vacuum tube, such as flicker noise and unexpected low-frequency perturbations, are more difficult to suppress. This is because they are generated by the flatness and compositions of a cathode's coatings [17] and ripples from a bias [18]. In addition, slow time-varying perturbations deteriorate the locking performance and cause phase jitters and frequency chirps in the output of the injection-locked system [19], [20].

To simplify the power-combining system and improve the output quality, we propose a novel power-combining system with dual-way injection-locked MGTs based on an asymmetric H-plane tee and closed-loop phase compensation (CLPC). According to the theoretical derivation of the proposed method, the correlations among the combining efficiencies, phase differences, locking bandwidths, and coupling strengths are theoretically analyzed, and the mechanism of noise inhibition is theoretically explained. Moreover, we developed an experimental system for validation. The simplified schematic of the proposed dual-way MGT power-combining system is presented in Fig. 1. Owing to the coupling between the input branches of the asymmetric H-plane tee, MGT #2 can be

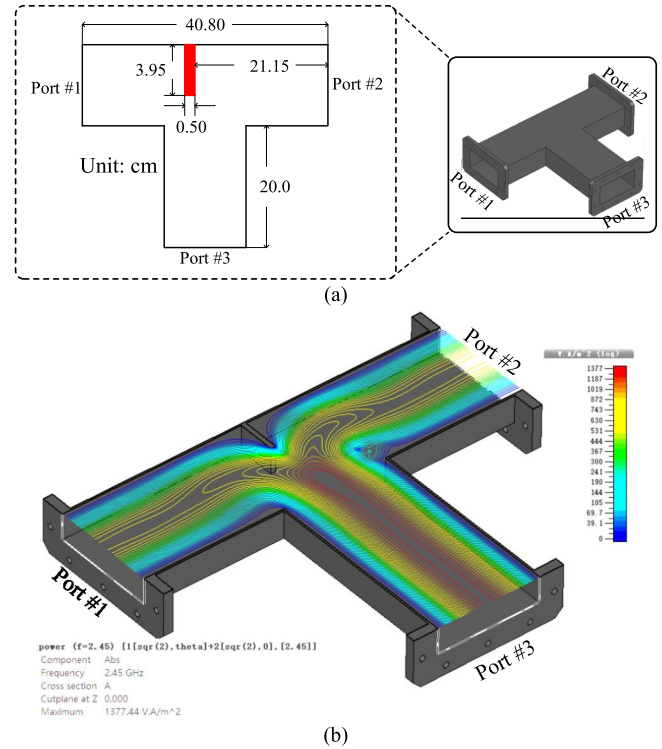


Fig. 2. (a) Physical dimensions of the designed asymmetric H-plane tee. (b) Power flow when the phase difference between the inputs is optimal in the CST environment.

preliminarily synchronized by MGT #1. Both MGTs will be simultaneously locked with the external reference signal, whereas only MGT #1 is locked by an external injection. The optimal power-combining efficiency is then obtained using frequency tuning of the injected signal. Furthermore, implementing only one CLPC subsystem can automatically compensate for the phase fluctuation of the combined output. Thus, the near-carrier noise of the combined output had a strong suppression of more than 20 dB from 10 to 10^3 Hz, and the phase jitter was limited to approximately $\pm 0.5^\circ$. The quality of the combined output was almost identical to that of the external reference signal, and the measured results qualitatively agreed with the theoretical estimations.

II. ASYMMETRIC H-PLANE TEE

The asymmetric H-plane tee was designed using the WR430 waveguide and an aluminum alloy; its cross-sectional dimensions are presented in Fig. 2(a). The characteristics of asymmetry were introduced and determined by optimizing the position and length of the metal plane, which is symbolized in Fig. 2(a) by a red block. The modeling and electromagnetic simulation were accomplished using *CST Studio Suite*® software, as shown in Fig. 2(a) and (b).

The simulation and measurement results of the scattering parameters and phase differences are shown in Fig. 3(a) and (b), respectively. Let us focus on the measured data at 2.45 GHz. $|S_{13}|$ and $|S_{23}|$ are -3.18 and -2.94 dB, respectively, and $|S_{21}|$ equals -4.47 dB, which is approximately 1.5 dB higher than the standard H-plane tee [9]–[12], [14]. $|S_{11}|$ and $|S_{22}|$ equal -7.39 and -7.80 dB,

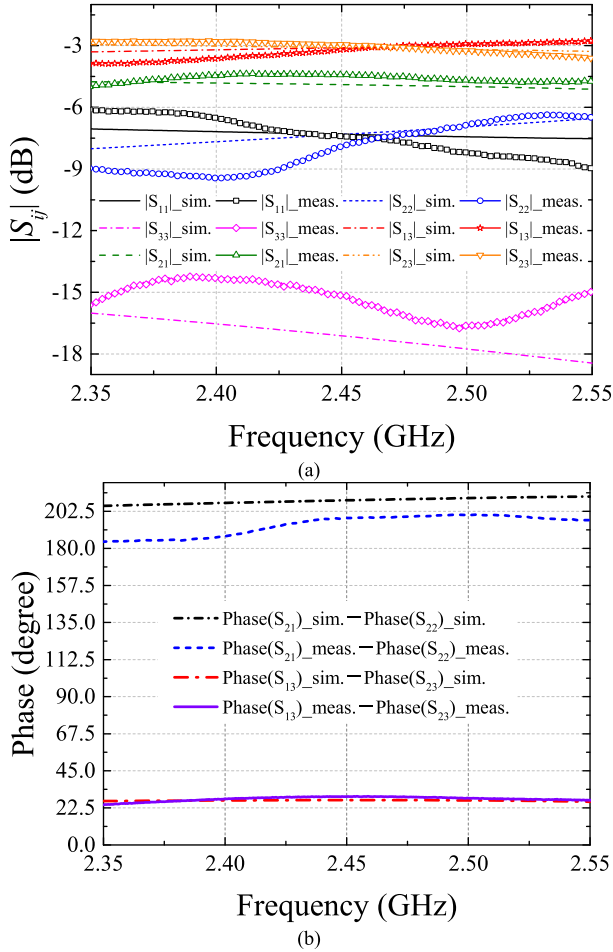


Fig. 3. Simulated and measured asymmetric H-plane tee. (a) Scattering parameters. (b) Phase differences.

respectively, which indicates a decrease of about 1.5 dB from the standard H-plane tee. $|S_{33}|$ of Port #3 is -15.22 dB. The phase difference between S_{21} and S_{22} is $\text{Phase}(S_{21}) - \text{Phase}(S_{22}) = 198.50^\circ$, and that between S_{13} and S_{23} is $\text{Phase}(S_{13}) - \text{Phase}(S_{23}) = 29.38^\circ$. A comparison of the measured and simulated results is presented in Table I. The deviations between the measured scattering parameters and simulated results were caused by fabrication error and a slight mismatch of the waveguide connections; however, such errors are small and acceptable.

Additionally, the power flow in the simulated environment is shown in Fig. 2(b), where the maximum combining efficiency of the asymmetric H-plane tee is 97.4% at the input setup of $P_{\text{port}\#1} = P_{\text{port}\#2}$, $\text{Phase}(S_{13}) - \text{Phase}(S_{23}) = 27.22^\circ$.

III. THEORETICAL ANALYSIS

As depicted in Fig. 1, when an H-plane tee is used as a power combiner, its signal streams can be determined from the following scattering matrix:

$$[V_i^-] = [S]_{\text{H-Tee}} [V_i^+] = \begin{bmatrix} |S_{11}|e^{j\alpha_1} & |S_{12}|e^{j\beta_1} & |S_{13}|e^{j\chi_1} \\ |S_{21}|e^{j\beta_2} & |S_{22}|e^{j\alpha_2} & |S_{23}|e^{j\zeta_1} \\ |S_{31}|e^{j\chi_2} & |S_{32}|e^{j\zeta_2} & 0 \end{bmatrix} \times \begin{bmatrix} |V_1^+|e^{j\theta_1} \\ |V_2^+|e^{j\theta_2} \\ 0 \end{bmatrix} \quad (1)$$

TABLE I
COMPARISON OF THE SIMULATED AND MEASURED RESULTS AT 2.45 GHz

Parameter	Simulation	Measurement
$ S_{13} $	-3.10 dB	-3.18 dB
$ S_{23} $	-3.10 dB	-2.94 dB
$ S_{21} $	-4.90 dB	-4.47 dB
$ S_{11} $	-7.31 dB	-7.39 dB
$ S_{22} $	-7.32 dB	-7.80 dB
$ S_{33} $	-17.11 dB	-15.22 dB
$\text{Phase}(S_{21}) - \text{Phase}(S_{22})$	208.59°	198.50°
$\text{Phase}(S_{13}) - \text{Phase}(S_{23})$	27.22°	29.38°

where V_i^+ and V_i^- are the input and output voltages, respectively; α_i , β_i , χ_i , and ζ_i are the phases of the H-plane tee combiner; and θ_i is the phase of the input signal. The formula for the output signals is

$$\begin{bmatrix} V_1^- \\ V_2^- \\ V_3^- \end{bmatrix} = \begin{bmatrix} |V_1^+| |S_{11}| e^{j(\alpha_1 + \theta_1)} + |V_2^+| |S_{12}| e^{j(\beta_1 + \theta_2)} \\ |V_1^+| |S_{21}| e^{j(\beta_2 + \theta_1)} + |V_2^+| |S_{22}| e^{j(\alpha_2 + \theta_2)} \\ |V_1^+| |S_{31}| e^{j(\chi_2 + \theta_1)} + |V_2^+| |S_{32}| e^{j(\zeta_2 + \theta_2)} \end{bmatrix}. \quad (2)$$

Obviously, V_1^- and V_2^- are the mutual coupling voltages; however, V_1^- will be absorbed by the dummy load #1 in the proposed system. The power-combining efficiency in the H-plane tee is determined as follows:

$$\eta_{\text{combiner}} = 100\% \times \frac{[|V_1^+| |S_{31}| + |V_2^+| |S_{32}| e^{j(\zeta_2 - \chi_2 + \theta_2 - \theta_1)}]^2}{V_1^{+2} + V_2^{+2}}. \quad (3)$$

Next, we consider the characteristics of the asymmetric H-plane tee of the proposed power-combining system. Three locking conditions are of interest in this study.

A. Coupling Injection-Locking Condition

V_2^- is considered the signal injected into MGT #2 when external injection is absent. Then, the injection ratio of the coupling is determined as follows:

$$\xi_{21} = \frac{|V_1^+| |S_{21}|}{|V_2^+|} + |S_{22}| e^{j(\alpha_2 - \beta_2 + \theta_2 - \theta_1)}. \quad (4)$$

When coupling injection-locking (CIL) occurs, the steady locking condition [21], [22] can be determined using

$$\omega_1 - \omega_2 = \frac{\omega_2 \xi_{21}}{2Q_{\text{ext}}} \sin(\theta_2 - \theta_1) \quad (5)$$

where ω_1 and ω_2 are the operating frequencies of MGT #1 and MGT #2, respectively, and Q_{ext} is the external quality factor of the MGT. For simplicity, we assume that the Q_{ext} values of the MGTs are the same. When locking occurs, the frequency of MGT #2 is synchronized with that of MGT #1. Then, the phase difference between the two inputs is deduced as follows:

$$y = \sin^{-1} \left[\frac{2Q_{\text{ext}} |V_2^+| x}{|V_1^+| |S_{21}| + |V_2^+| |S_{22}| \cos(\alpha_2 - \beta_2 + y)} \right]. \quad (6)$$

In the transcendental (6), $y = \theta_2 - \theta_1$ and $x = (\omega_1 - \omega_2)/\omega_2$. Ideally, the values of Q_{ext} , $|S_{21}|$, $|S_{22}|$, and $\alpha_2 - \beta_2$ are

determined by the practical components and are perceived to be constants. If the input strengths are equal, that is, $|V_1^+| = |V_2^+|$, y can be altered only by varying x .

B. EIL After Preliminary CIL

As MGT #2 preliminarily synchronized with MGT #1, an external injection was applied to MGT #1 via a circulator. The locking condition of MGT #1 is written as

$$\omega_{\text{inj}} - \omega_1 = \frac{\omega_1 \rho_{\text{inj}}}{2Q_{\text{ext}}} \sin \phi \quad (7)$$

where ω_{inj} is the frequency of the reference signal and ρ_{inj} is the external injection ratio that equals the square root of the power ratio between the external reference and the output of MGT #1, that is, $\rho_{\text{inj}} = (P_{\text{inj}}/P_{\text{MGT}\#1})^{1/2}$. Additionally, ϕ is the phase difference between the external reference and MGT #1, that is, $\phi = \theta_{\text{inj}} - \theta_1$. As CIL and external injection-locking (EIL) occur simultaneously, the phase relationships are given as follows:

$$\theta_2 = C_1 + \theta_1 \quad (8)$$

$$\theta_{\text{inj}} = C_2 + \theta_1 \quad (9)$$

where C_1 and C_2 are constants. Certainly, the variations in θ_1 are determined by θ_{inj} . Substituting (8) into (9), we obtain

$$\theta_2 = C_1 - C_2 + \theta_{\text{inj}}. \quad (10)$$

Equations (9) and (10) clearly explain how θ_1 and θ_2 are controlled simultaneously by the variations in θ_{inj} . Thus, the phase of the coherent combined output will be fully controlled by only one phase-controllable external injection.

Substituting (7) into (6), the x value in (6) is updated as $x' = (\omega_{\text{inj}} - \omega_1)/\omega_1$ when the preliminary CIL system is locked by the frequency-tuning external reference signal. In addition, the variation in $\theta_2 - \theta_1$ is valid only at the intersection of the CIL and EIL bandwidths:

$$\Delta\omega_{\text{valid}} = \left[\omega_1 - \frac{\omega_1 \zeta_{21}}{2Q_{\text{ext}}}, \omega_1 + \frac{\omega_1 \zeta_{21}}{2Q_{\text{ext}}} \right] \cap \left[\omega_1 - \frac{\omega_1 \rho_{\text{inj}}}{2Q_{\text{ext}}}, \omega_1 + \frac{\omega_1 \rho_{\text{inj}}}{2Q_{\text{ext}}} \right]. \quad (11)$$

Within the overlapped locking region, the frequencies of the MGTs will track the injected frequency as $\omega_{\text{inj}} = \omega_1 = \omega_2$. We assume that the preliminary CIL frequency is 2.4495 GHz and that the input voltages are equal, that is, $|V_1^+| = |V_2^+|$. Assuming that the external quality factor is 50, we used the measured data of the designed asymmetric H-plane tee presented in Table I to numerically calculate (3), (4), and (6). The numerical results are shown in Fig. 4(a)–(c), in which the colored bricks represent the scopes of phase adjustment with different external injection ratios. The shadow-filled brick symbolizes the invalid phase control region, where the injected frequency is beyond the couple-locking bandwidth. These results indicate the relationships among the phase differences of the inputs, scope of frequency tuning, coupling injection ratio, and combined efficiency of the asymmetric H-plane tee. By considering a 0.1-dB insertion loss and $\gamma = 29.38^\circ$, the optimal efficiency of the used asymmetric H-plane tee

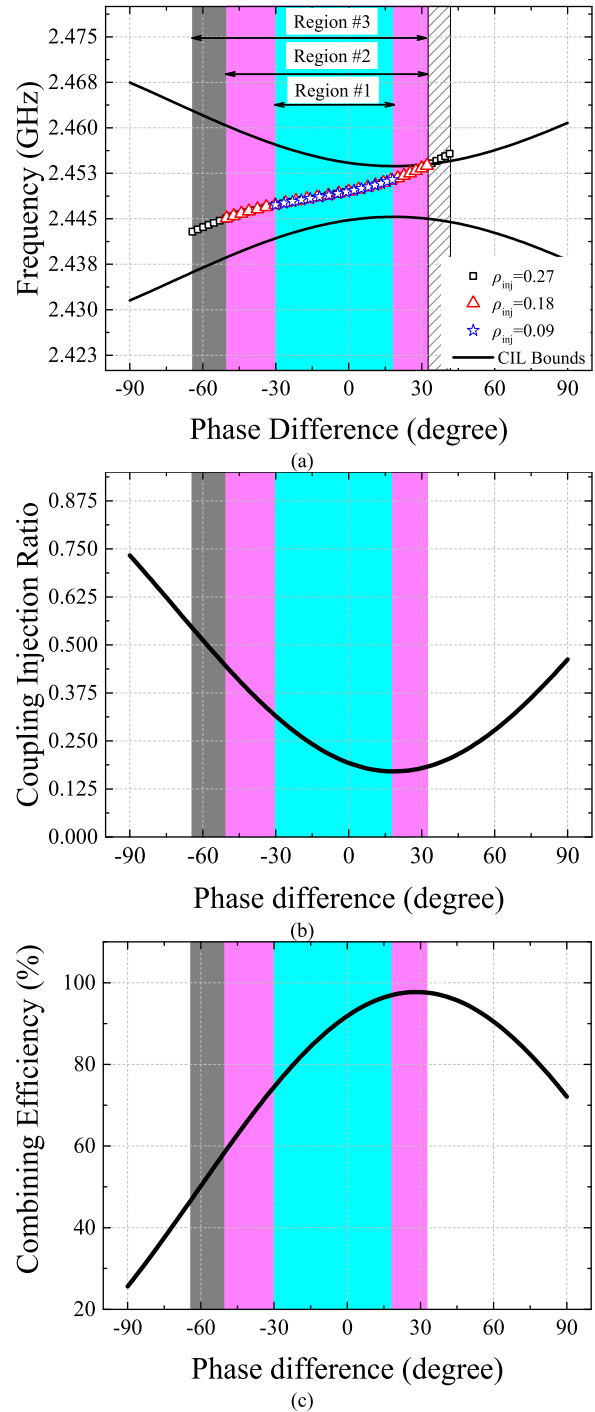


Fig. 4. Mapping relationships among the phase differences of the inputs, (a) frequency sweep scope, (b) coupling injection ratio, and (c) combining efficiency.

η_{asym} reaches 97.7% at 2.4533 GHz when $\rho_{\text{inj}} = 0.18$. If $\rho_{\text{inj}} = 0.09$, the frequency-tuning scope is narrowed down, and the phase-adjustable scope is insufficient for the optimal combined efficiency, in which the maximum frequency can reach only 2.4517 GHz. The extended frequency sweep (if $\rho_{\text{inj}} = 0.27$) will become invalid when the estimated EIL bandwidth exceeds the CIL region, as indicated by the shadow-filled brick in Fig. 4(a). Moreover, a higher ρ_{inj} broadens the power control scope of the combined output power.

C. Noise Suppression Contribution by Closed-Loop Phase Compensation

Using the theory derived by Chang *et al.* [23], the injection-locked MGT output noise level $|\delta\tilde{\theta}_{\text{OUT}}(\omega_m)|^2$ is written as follows:

$$\begin{aligned} |\delta\tilde{\theta}_{\text{OUT}}(\omega_m)|^2 &= |\delta\tilde{\theta}_{\text{MGT}}(\omega_m)|^2 \frac{(\omega_m/\omega_{3\text{dB}})^2}{\rho^2 \cos^2 \phi' + (\omega_m/\omega_{3\text{dB}})^2} \\ &+ |\delta\tilde{\theta}_{\text{inj}}(\omega_m)|^2 \frac{\rho^2 \cos^2 \phi'}{\rho^2 \cos^2 \phi' + (\omega_m/\omega_{3\text{dB}})^2} \end{aligned} \quad (12)$$

where $\delta\tilde{\theta}_{\text{MGT}}(\omega_m)$ and $\delta\tilde{\theta}_{\text{inj}}(\omega_m)$ are the noises of the free-running MGT and reference signal, respectively; ϕ' is the steady phase difference between the MGT's output and the reference signal; ω_m is the frequency that migrated from the carrier; and the locking bandwidth is $2\rho\omega_{3\text{dB}}$.

As previously mentioned, MGT #2 was preliminarily locked via coupling from MGT #1. We consider that the noise levels of the two free-running MGTs are equal. Therefore, the output noise of the CIL system cannot be improved based on (12): $\delta\tilde{\theta}_{\text{CIL}}(\omega_m) = \delta\tilde{\theta}_{\text{MGT}\#1}(\omega_m) = \delta\tilde{\theta}_{\text{MGT}\#2}(\omega_m)$. Similarly, the phase noise of the EIL output $\delta\tilde{\theta}_{\text{EIL}}(\omega_m)$ can be deduced by substituting the phase noise of the external reference $\delta\tilde{\theta}_{\text{inj}}(\omega_m)$ into (12).

In the CLPC system shown in Fig. 5(a), the mixer is used as a phase detector. The intermediate-frequency (IF) output signal of the mixer has a constant voltage when the RF inputs (combined output) and local oscillator (LO) are coherent. The ideal output voltage can be written as follows:

$$V_{\text{IF}} = V_0 \cos(\theta_{\text{RF}} - \theta_{\text{LO}}) \quad (13)$$

where V_0 is a constant determined by the internal network characteristics of the mixer and the power levels of the inputs.

When near-carrier noise exists, low-frequency phase fluctuation $\delta\theta$ occurs in the relative phase, and the IF output signal can be rewritten as

$$V'_{\text{IF}} = V_0 \cos(\theta' + \delta\theta) \quad (14)$$

where θ' is a constant. Considering the frequency-domain solution of (14) and ignoring the dc component, the unilateral frequency-domain expression of (14) is written as $\delta\tilde{\theta}_{\text{IF}}(\omega_m)$.

In the noise flow of the closed-loop control system [Fig. 5(b)], the ultimate noise level is deduced by superposing the noises of each component in the feedback loop [24] when the CLPC is turned on, and the system enters the equilibrium condition. Then, the ultimate output noise is given by

$$\begin{aligned} \delta\tilde{\theta}_{\text{ULT}}(\omega_m) [1 + K_{\text{IF}} F_L(s) F_P(s)] \\ = \delta\tilde{\theta}_{\text{EIL}}(\omega_m) + \delta\tilde{\theta}_{\text{IF}}(\omega_m) F_L(s) F_P(s) \\ + [\delta\tilde{\theta}_L(\omega_m) + \delta\tilde{\theta}_P(\omega_m)] F_P(s) \\ + \delta\tilde{\theta}_{\text{REF}}(\omega_m) F_P(s). \end{aligned} \quad (15)$$

In (15), K_{IF} , $F_L(s)$, and $F_P(s)$ are the transfer functions of the mixer, active low-pass filter, and analog phase shifter, respectively; and $\delta\tilde{\theta}_{\text{REF}}(\omega_m)$, $\delta\tilde{\theta}_{\text{EIL}}(\omega_m)$, $\delta\tilde{\theta}_{\text{IF}}(\omega_m)$, $\delta\tilde{\theta}_P(\omega_m)$, and $\delta\tilde{\theta}_L(\omega_m)$ are the noises of the reference signal, EIL output, IF output, phase shifter, and active low-pass filter, respectively.

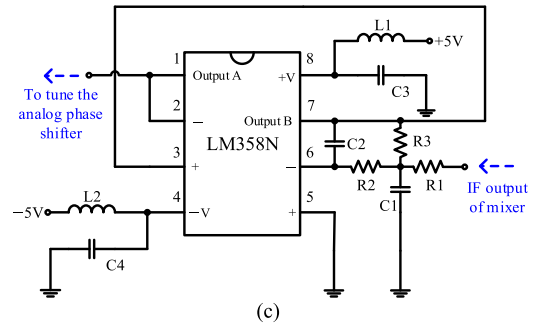
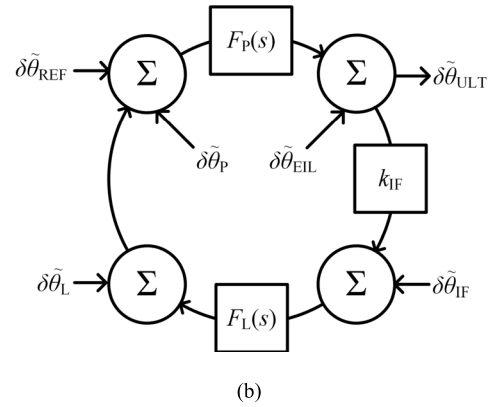
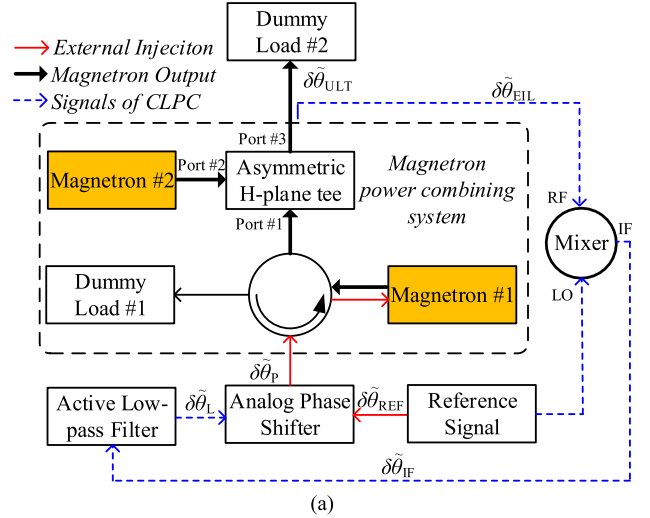


Fig. 5. (a) Configuration of the CLPC system. (b) Noise flow diagram of the CLPC. (c) Schematic of the active low-pass filter.

In the proposed CLPC system, $\delta\tilde{\theta}_{\text{EIL}}(\omega_m)$ is unique and is generated from the MGT. The IF output of the mixer is extracted by phase comparison between the combined and reference signals. Therefore, $\delta\tilde{\theta}_{\text{IF}}(\omega_m)$ is proportional to $\delta\tilde{\theta}_{\text{EIL}}(\omega_m)$, and $\delta\tilde{\theta}_L(\omega_m)$ and $\delta\tilde{\theta}_P(\omega_m)$ are introduced chiefly by the perturbation of the corresponding bias and the nonlinearity of the internal circuit. In addition, $\delta\tilde{\theta}_{\text{REF}}(\omega_m)$ is independent of $\delta\tilde{\theta}_{\text{EIL}}(\omega_m)$, $\delta\tilde{\theta}_P(\omega_m)$, and $\delta\tilde{\theta}_L(\omega_m)$. Herein, the correlation between these noises can be expressed as follows:

$$\begin{cases} |\delta\tilde{\theta}_{\text{EIL}}(\omega_m) \cdot \delta\tilde{\theta}_{\text{IF}}^*(\omega_m)| = S |\delta\tilde{\theta}_{\text{EIL}}(\omega_m) \cdot K_{\text{IF}} \delta\tilde{\theta}_{\text{EIL}}^*(\omega_m)| \\ \delta\tilde{\theta}_{\text{EIL}}(\omega_m) \perp \delta\tilde{\theta}_P(\omega_m) \perp \delta\tilde{\theta}_L(\omega_m) \perp \delta\tilde{\theta}_{\text{REF}}(\omega_m) \end{cases} \quad (16)$$

where S is the scaling factor determined by the attenuation of the mixer and symbolizes the correlated strength between

$\delta\tilde{\theta}_{\text{IF}}(\omega_m)$ and $\delta\tilde{\theta}_{\text{EIL}}(\omega_m)$. For simplicity, we assume that the IF output of the mixer is linearly amplified by the active low-pass filter to drive the ideal analog phase shifter. Therefore, the ultimate phase noise can be written as follows:

$$\begin{aligned} & |\delta\tilde{\theta}_{\text{ULT}}(\omega_m)|^2 \\ &= |1 - H(s)|^2 |\delta\tilde{\theta}_{\text{EIL}}(\omega_m)|^2 \\ &+ \frac{[F_L^*(s)F_P^*(s) + F_L(s)F_P(s)]K_{\text{IF}}S|\delta\tilde{\theta}_{\text{EIL}}(\omega_m)|^2}{|1 + K_{\text{IF}}F_L(s)F_P(s)|^2} \\ &+ |H(s)|^2 \left| \frac{\delta\tilde{\theta}_{\text{IF}}(\omega_m)}{K_{\text{IF}}} \right|^2 + |H(s)|^2 \left| \frac{\delta\tilde{\theta}_{\text{REF}}(\omega_m)}{K_{\text{IF}}F_L(s)} \right|^2 \end{aligned} \quad (17)$$

where

$$H(s) = \frac{K_{\text{IF}}F_L(s)F_P(s)}{1 + K_{\text{IF}}F_L(s)F_P(s)}$$

and

$$F_L(s) = -\frac{1}{s^2 + s\frac{1}{C_1}\left(\frac{1}{R_1} + \frac{1}{R_2} + \frac{1}{R_3}\right) + \frac{1}{C_1C_2R_2R_3}}.$$

The transfer functions of the mixer and analog phase shifter are determined to be $K_{\text{IF}} = 2 \times 10^{-3} \text{ V}^\circ$ and $F_P(s) = -K_p/(1 + sT)$, respectively. Here, $K_p = 30^\circ/\text{V}$ is the phase sensitivity, and T is the time constant at the typical level of 100 ns. Both the initial phase noises followed the ideal $1/f^2$ dependence [23], [24]: $|\delta\tilde{\theta}_{\text{MGT}}(\omega_m)|^2 = 2\pi \cdot 10^2/(\omega_m)^2$ and $|\delta\tilde{\theta}_{\text{inj}}(\omega_m)|^2 = 2\pi \cdot 10^{-2}/(\omega_m)^2$. Additionally, we omitted the signal dispersion and the noises of the phase shifter and the active low-pass filter in the following calculations. The value of S is 0.25 (6-dB conversion loss of the used mixer). The inverted active low-pass amplifier is schematically displayed in Fig. 5(c). The parameters of the used components are given as $R_1 = 100 \ \Omega$, $R_2 = 330 \ \Omega$, $R_3 = 470 \ \text{k}\Omega$, $C_1 = C_2 = 10 \ \text{pF}$, $C_3 = 200 \ \mu\text{F}$, and $L_1 = L_2 = 4700 \ \mu\text{H}$. The phase noises of the proposed system are then theoretically computed by substituting the above parameters into (12) and (17).

In Fig. 6(a) and (b), when the locking conditions are satisfied, which include the EIL condition and the CLPC, both the phase noises will be suppressed. As shown in Fig. 6(a), with the various ρ_{inj} values, the phase noise curves follow the curve of reference at the frequency band ranging from 10 to 10^3 Hz. When the frequency migrates from 10^3 to 10^6 Hz, the noise level is gradually suppressed by increasing ρ_{inj} . Considering the effect of CLPC [Fig. 6(b)], the noise levels are further suppressed when the migrated frequency is lower than 1.28 MHz, which is the cutoff frequency of the active low-pass filter, and the suppression is up to 11 dB. By increasing the injection strength from 0.1 to 0.2, the noise level can be suppressed, but the changes are not noticeable.

IV. EXPERIMENTAL SYSTEM

A block diagram of the dual-way microwave power-combining system proposed in this article is shown in Fig. 7(a). In the photograph of the system, as shown in Fig. 7(b), two commercial CW 2.45-GHz MGTs (2M167B-M32, Panasonic) are connected to the ports of the H-branch of the asymmetric H-plane tee. Both the MGTs

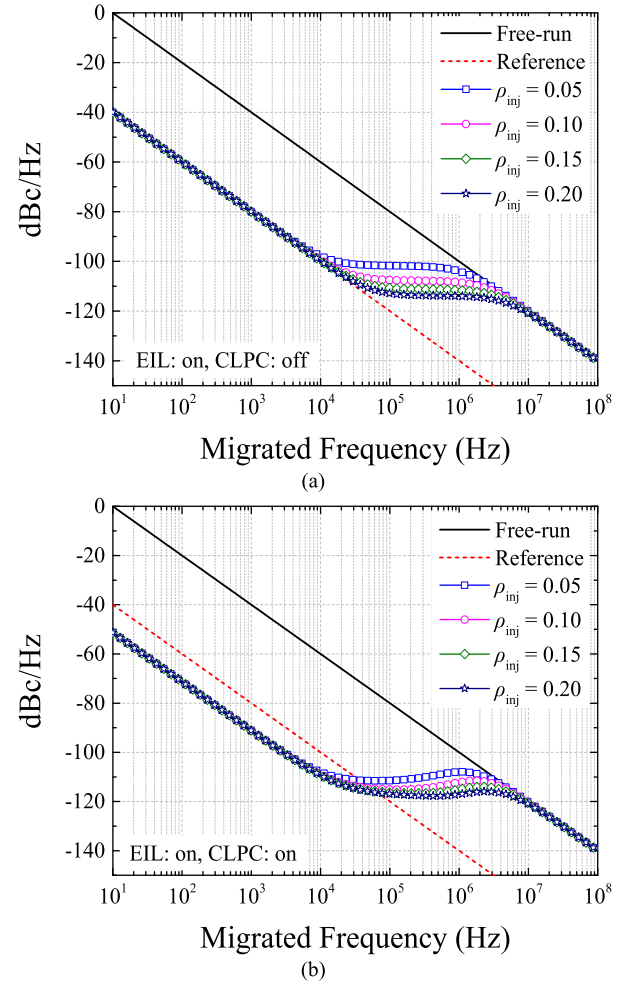


Fig. 6. (a) Characteristics of the relative output phase noise of the free-running oscillator, external injection source, and EIL magnetron. (b) Characteristics of the relative output phase noise of the free-running oscillator, external injection source, and EIL magnetron when the CLPC is activated.

are powered by economic power supplies (WepeX 1000B-TX, Megmeet) with an improved anode voltage of approximately 1%. Additionally, the filament current can be switched off to decrease the spurious noise of the free-running output. A microwave source (E4421B, Agilent) and a power amplifier (CA2450BW100-4547M-C, R&K) provide the reference signal to inject MGT #1 via two circulators (WUC-022K8, insertion loss: 0.3 dB at 2.45GHz, Nihon Koshuha). The coupling power from Port #2 to Port #1 and the combined power are absorbed by the dummy load, and the signal information is sampled by the couplers. The power data are measured using two power meters (A1914A, Agilent and E4419B, Agilent). The spectra and phase noises are visualized and recorded by a signal analyzer (N9010A, Agilent). The phase jitter and the phase difference between the reference signal and the combined signal are monitored and recorded via a vector network analyzer (VNA) (E8722ES, Agilent). The operating anode voltage and current are visualized using an oscilloscope (TDS-3054, Tektronix) with a voltage probe (P6015A, Tektronix) and a current probe module (TCP312A and TPC A300, Tektronix).

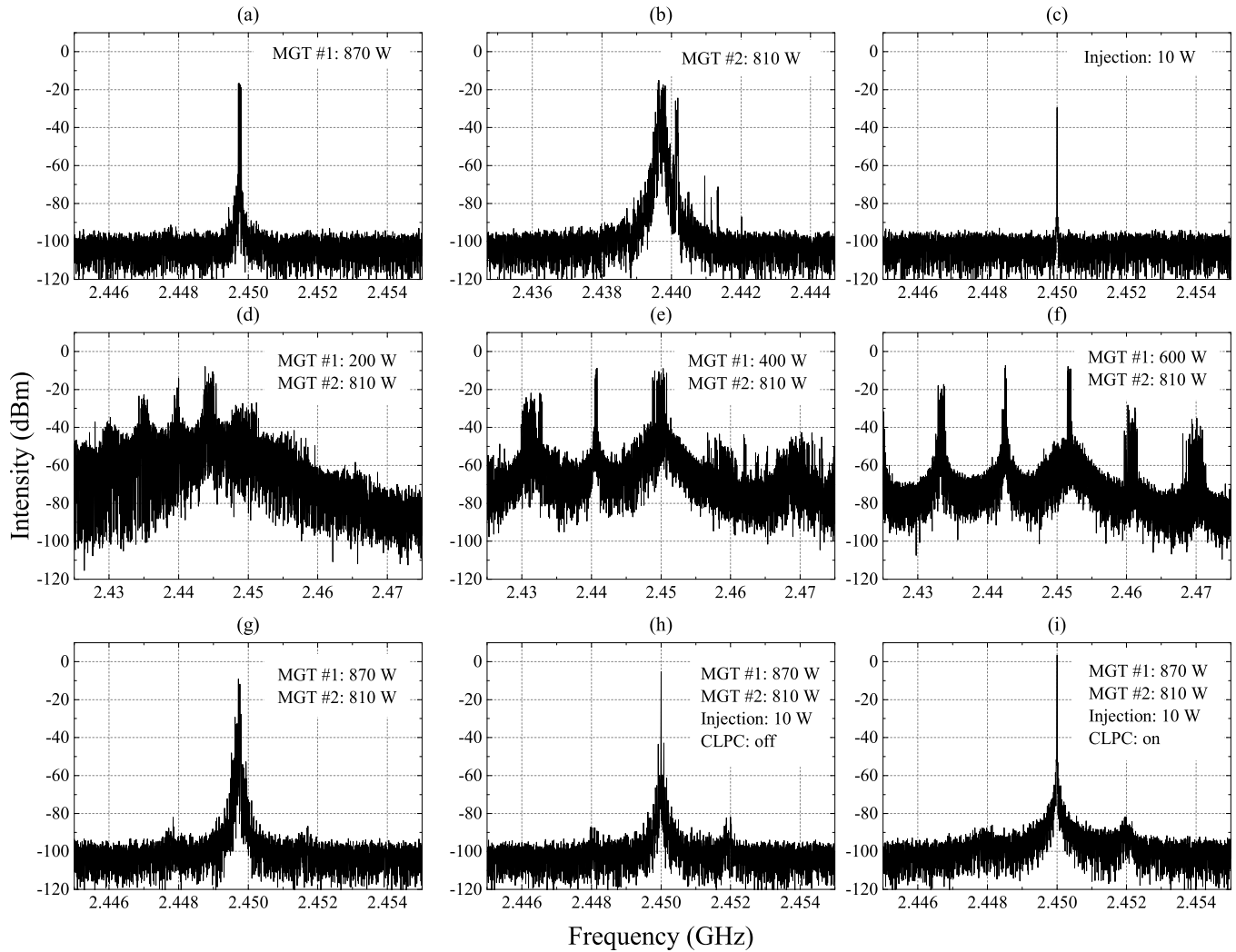


Fig. 8. Spectra of the proposed system in different conditions. The resolution bandwidth is 3 kHz, and the video bandwidth is 3 kHz.

monitored frequency area, and the floor noise increased. The system in this condition was useless because of its extremely poor output. This spurious outcome causes unstable output power and increases the risk of electromagnetic interference with other electrical devices that operate at adjacent frequency bands.

When the power of MGT #1 increased to 870 W, CIL occurred by the coupling power from MGT #1. The output frequency of MGT #2 was approximately 2.4497 GHz, as shown in Fig. 8(g), but the noise was still distributed near the carrier. The CIL technique demonstrated that the external injection was unnecessarily applied [9]. Nevertheless, when a noisy MGT is used to synchronize other MGTs, the locking state is temporal, which creates intermodulation products and dramatic fluctuations in the output [9], [15], [19], [20].

In the presence of a 2.45-GHz 10-W external reference signal injected into MGT #1, EIL occurred, and the signal quality was significantly improved, as shown in Fig. 8(h).

By tuning the injected frequency to 500-kHz intervals, we optimized the combined power and the corresponding combining efficiency of the used asymmetric H-plane tee η_{asym} . This

optimization of η_{asym} is clear in Fig. 9(a). It is interesting to note that the trend of the η_{asym} variation with respect to the injected frequency was monotonic; high combining efficiencies were obtained in the upper regions of the locking bandwidth. The high injection ratio contributed to the wide locking bandwidth of the combining system. The locking bandwidth reached 6.1 MHz with 25-W injection power (injection ratio ρ_{inj} near 0.17), but the bandwidth dropped to 1.0 MHz when the injection power was 1 W (ρ_{inj} near 0.03). The locking ranges, power-adjustable scopes, and variation in the combining efficiencies with different external injection strengths are given in Table II; the maximum combined power P_{com} and η_{asym} reached 1.58 kW and 95.7%, respectively.

In the case of the optimal η_{asym} (95.7%), the driven powers of the MGTs were 1350 and 1340 W, respectively, as calculated using the measured anode voltage and current of the MGTs. Even with a low injection strength (e.g., 1 W), the optimal combining efficiency still exceeded 90%. The variations in η_{asym} and the output power of the two MGTs in the presence of a 25-W external injection are shown in Fig. 9(b). At the lower combining efficiency region, which

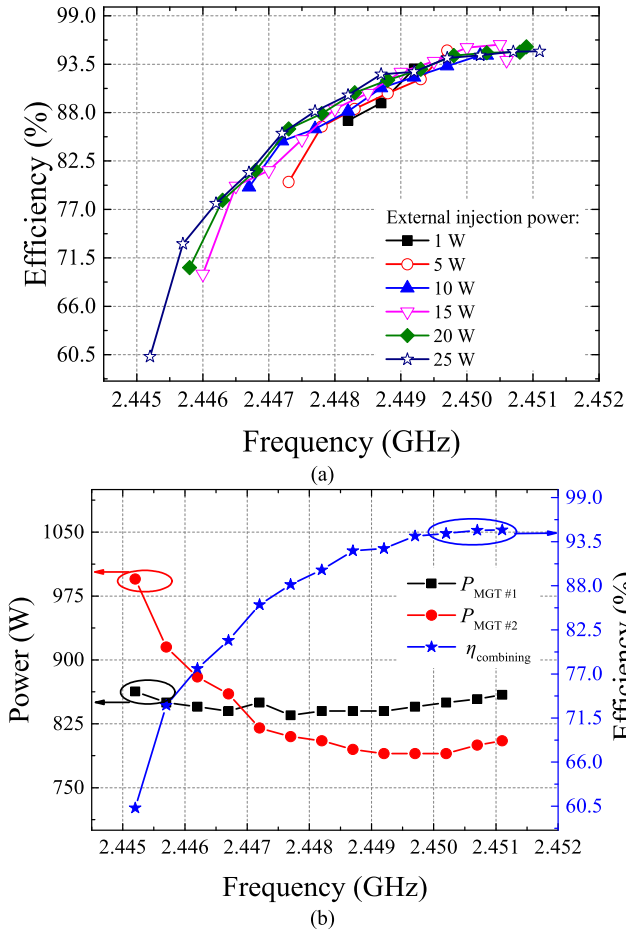


Fig. 9. (a) Measured power-combining efficiency with respect to the varied external injection frequency. (b) Power variations of two magnetrons and the combining efficiency with respect to the tuned frequency.

TABLE II
MEASURED DATA OF THE COMBINING OUTPUT

ρ_{inj}	Locking Scope (GHz)	Scope of P_{com} (kW)	Scope of η_{asym} (%)
0.034	2.4482–2.4492	1.45–1.52	87.1–93.0
0.076	2.4473–2.4497	1.37–1.53	80.1–95.0
0.107	2.4467–2.4503	1.36–1.55	79.5–94.5
0.131	2.4460–2.4506	1.24–1.57	69.7–95.7
0.152	2.4458–2.4509	1.26–1.58	70.4–95.5
0.170	2.4452–2.4511	1.12–1.58	60.3–95.0

ranged from 2.4452 to 2.4472 GHz, the detected output power of MGT #2 dropped quite dramatically; however, that of MGT #1 dropped only marginally. This phenomenon was caused by the coupling power from MGT #1 to MGT #2 and was transmitted along with the original power of MGT #2. This implies that the received coupling power of MGT #2 decreased upon increasing the injected frequency, which confirms our theoretical prediction [see Fig. 4(b)]. Moreover, the results are also in agreement with those reported in [25]–[27].

The maximum η_{asym} value of the numerical calculation closely approximated the prediction of the full-wave simulation obtained using the CST software, at 97.4%. However,

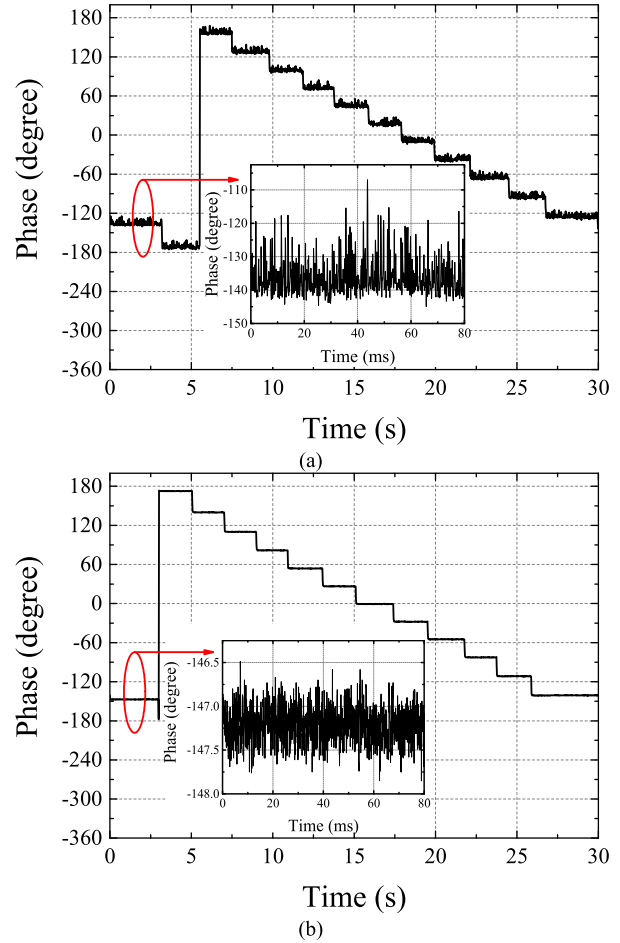


Fig. 10. Phase adjustment of the combining signal (a) when the EIL is turned on and (b) when both the EIL and CLPC are turned on.

the measured maximum η_{asym} of the practical system was slightly lower, at 95.7%, indicating a difference of only 2%. Additionally, the simulated variation in η_{asym} with respect to frequency tuning [Fig. 4(c)] was monotonic and qualitatively agreed with the measurement results [Fig. 9(a)].

When the maximum combining efficiency was obtained at the optimal frequency with an external injection power of 10 W, the analog phase shifter was activated by a dc voltage ranging from 0 to 12 V with intervals of 1 V. The phase of the combined output was then controlled by adjusting the phase of only one external injection. The phase difference between the reference signal and the combined output was monitored using a VNA at a constant frequency. As shown in Fig. 10(a), the phase control of the combined output was valid with a scope of approximately 360°.

Fig. 8(h) shows that microphonic noise remained around the carrier. As shown in Fig. 10(a), the time-varying components in the phase were present when both MGTs were locked by the external reference signal. These components were also clear in the VNA; the phase jitter is shown in detail in Fig. 10(a) at a resolution of 1601 samples in 80 ms, where the peak-to-peak value of the phase jitter exceeded 20°. The corresponding phase noise curves are plotted in Fig. 12(a). When EIL occurred, the noise levels were significantly suppressed from 10 to 10⁶ Hz. When the migrated frequency was increased

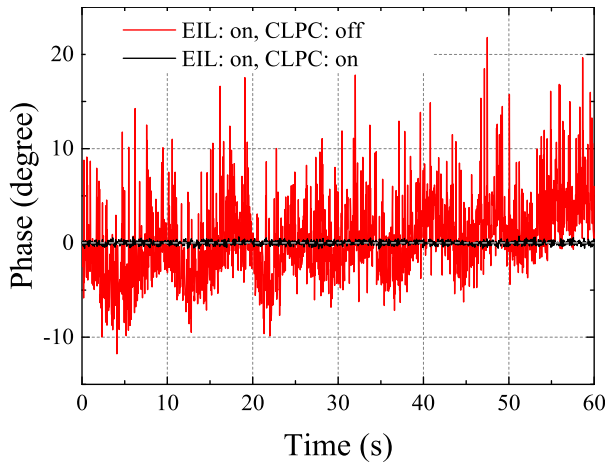


Fig. 11. Long-term comparison of phase jitters. The white dashed line is the x -axis of the chart.

to 10^7 Hz, the noise level was approximately equal to that of the free-running condition. Nevertheless, the near-carrier noise ranging from 10 to 10^3 Hz remained strong and could not be inhibited by increasing the injection strength.

By activating the CLPC subsystem, the noise information originating from the IF port of the mixer was inverted and amplified to drive the analog phase shifter. Then, instantaneous compensation of phase fluctuation occurred, and the phase difference was minimized when the CLPC reached the equilibrium condition. As shown in Fig. 8(i), the near-carrier frequency components were eliminated, and their spectra were almost as sharp as the reference signal [Fig. 8(c)]. Fig. 10(b) shows that the phase adjustment had high purity when the CLPC was turned on. The peak-to-peak value of the phase jitter was closely approximated to $\pm 0.5^\circ$, and the elimination of phase perturbation was expressed by the suppression of the phase noise.

As shown in Fig. 12(b), the noise level ranging from 10 to 10^3 Hz was almost entirely eliminated when the external injection power was ≥ 5 W, and the maximum suppression strength was more than 20 dB relative to the EIL conditions. In the range of 10– 10^5 Hz, the phase noise curve of the proposed system's combined output almost overlapped with that of the reference signal. The results show strong purity in the MGT output, and the noise levels were remarkable (e.g., -61.0 dBc/Hz at 10 Hz, -80.9 dBc/Hz at 100 Hz, -91.6 dBc/Hz at 1 kHz, -97.9 dBc/Hz at 10 kHz, -113.9 dBc/Hz at 100 kHz, and -132.5 dBc/Hz at 1 MHz). However, the changes in the output noise curves were virtually indistinguishable from one another when the injection strengths were higher than 5 W. Under this condition, the proposed system can act as an element phase-controlled source for the phased-array application in which the element's output power exceeds the power limitation of a single MGT.

Fig. 11 shows a direct comparison of the 60-s recording phase jitters. The phase jitter of the EIL condition was dramatic, and the phase shift was visible. On the contrary, the phase curve was stable as a straight line with the collaborative operation of CLPC and EIL.

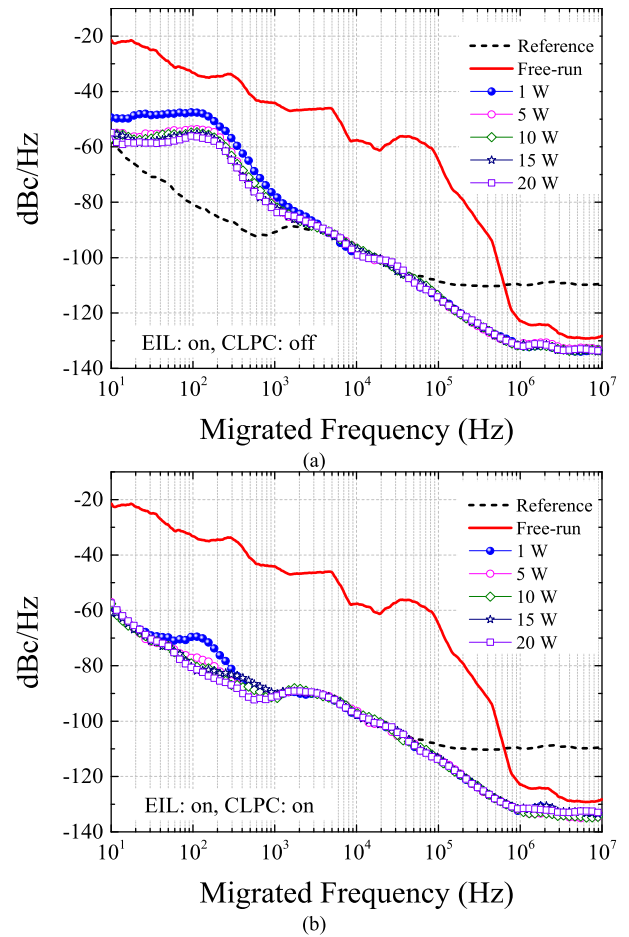


Fig. 12. Noise performances of combining the output with respect to the different external injection power. (a) EIL: on, CLPC: off; (b) EIL: on, CLPC: on.

In the above measurements, we investigated the noise improvement of the power-combining system with the CLPC. The EIL combined with the CLPC showed better output phase-noise suppression than that using only EIL. However, the measurement results cannot be directly compared with the computed results, which are more distorted, as shown in Fig. 12(a) and (b). The curves in Fig. 12(a) and (b) do not follow the $1/f^2$ dependence. Here, the simulations consider the noise of only the MGT. Noises contributed by the nonlinearity of the semiconductor in the active low-pass filter, mixer, analog phase shifter, and RF power amplifier are inevitable but are difficult to determine in our laboratory conditions. Factors such as the frequency-pushing effect, thermal drift, and perturbation of the load properties of the MGT system are more computationally complicated. Nevertheless, the noise was further suppressed at the near-carrier frequency band in both the computed and measured results. More importantly, it was possible to minimize the near-carrier frequency noises using the customized design of the CLPC subsystem in the injection-locked MGT system to achieve high stability. In that case, the noise behaviors were as close to the reference signal as possible. Additionally, the advantage of cost-saving is significant when only one CLPC subsystem is used to improve the dual-way MGTs simultaneously.

TABLE III

COMPARISON OF OUR MAGNETRON POWER-COMBINING SYSTEM WITH THOSE IN OTHER STUDIES BASED ON DUAL-WAY S-BAND MAGNETRONS

	Freq. (GHz)	ρ_{mj}	Phase control of the combining output	Phase jitter	Phase noise	η_{com} (%)	P_{out} (kW)
[8]	2.83	0.22	N/A	$\pm 1.0^\circ$ to $\pm 4.0^\circ$ during the pulse period	-	92.0	pulsed-type 49000
[9]	2.45	0.22	N/A	-	-	92.0	-
[10]	2.45	0.10	N/A	$\pm 6.0^\circ$	-50.0 dBc/Hz at 2 MHz	96.6	25.0
[11]	2.45	0.07	N/A	$\pm 0.9^\circ$	-65.0 dBc/Hz at 500 kHz	94.7	34.0
[13]	2.45	0.08	N/A	$\pm 2.0^\circ$	-35.0 dBc/Hz at 75 kHz	93.0	2.0
[14]	2.45	0.25	N/A	-	-	94.6	2.0
This work	2.45	0.13	0° – 360°	almost $\pm 0.5^\circ$	-61.0 dBc/Hz at 10 Hz, -80.9 dBc/Hz at 100 Hz, -91.6 dBc/Hz at 1 kHz, etc.	95.7	1.57

Table III gives a detailed comparison of the performances of the proposed system with the other S-band dual-way MGT power-combining systems. This is the first time that a high-efficiency microwave power-combining system has been developed with 0° – 360° phase control in the combined output; the systems developed in [8]–[11], [13], and [14] do not have this capability. Furthermore, the phase jitter and phase noise level of the proposed system are lower than those reported in [8], [10], [11], and [13].

VI. CONCLUSION

We proposed and experimentally investigated a novel microwave power-combining system with dual-way MGTs using an asymmetric H-plane tee and a single CLPC. When the asymmetric H-plane tee with asymmetric port characteristics was used in the system to achieve coupling locking, both MGTs were locked simultaneously using only one external injection. Optimal power-combining efficiency was achieved for the asymmetric H-phase tee using frequency tuning in the external injection, in which the maximum power-combining efficiency reached 95.7%. After the optimal combining efficiency was secured, the combined output was phase-controlled using only one phase shifter in which the control scope was 0° – 360° . To suppress the noise of the combined output, a CLPC subsystem was designed and validated. The near-carrier noise was largely eliminated, and the phase noise curves were extremely consistent with the external injection. Furthermore, the measurement results qualitatively agree with the theoretical estimation.

In the future, we hope to extend our proposed method to other high-power microwave source applications to further improve the output purity and reduce the system complexity.

REFERENCES

- [1] K. Kobashi, K. Nishimura, Y. Kawate, and T. Horiuchi, "Synthesis of diamonds by use of microwave plasma chemical-vapor deposition: Morphology and growth of diamond films," *Phys. Rev. B, Condens. Matter*, vol. 38, no. 6, p. 4067, Aug. 1988, doi: [10.1103/PhysRevB.38.4067](https://doi.org/10.1103/PhysRevB.38.4067).
- [2] Y. Zhang, D. K. Agrawal, J. Cheng, and T. Slaweck, "Microwave power absorption mechanism of metallic powders," *IEEE Trans. Microw. Theory Techn.*, vol. 66, no. 5, pp. 2107–2115, May 2018, doi: [10.1109/TMTT.2018.2804980](https://doi.org/10.1109/TMTT.2018.2804980).
- [3] W. C. Brown, "The history of power transmission by radio waves," *IEEE Trans. Microw. Theory Techn.*, vol. MTT-32, no. 9, pp. 1230–1242, Sep. 1984, doi: [10.1109/TMTT.1984.1132833](https://doi.org/10.1109/TMTT.1984.1132833).
- [4] N. Shinohara, "Beam control technologies with a high-efficiency phased array for microwave power transmission in Japan," *Proc. IEEE*, vol. 101, no. 6, pp. 1448–1463, Jun. 2013, doi: [10.1109/JPROC.2013.2253062](https://doi.org/10.1109/JPROC.2013.2253062).
- [5] T. Overett, D. B. Remsen, E. Bowles, G. E. Thomas, and R. E. Smith, "Phase locked magnetrons as accelerator RF sources," in *Proc. 12th IEEE Part. Accel. Conf.*, Mar. 1987, pp. 1464–1465.
- [6] A. C. Dexter *et al.*, "First demonstration and performance of an injection locked continuous wave magnetron to phase control a superconducting cavity," *Phys. Rev. Special Topics-Accel. Beams*, vol. 14, no. 3, pp. 1–11, Mar. 2011, doi: [10.1103/PhysRevSTAB.14.032001](https://doi.org/10.1103/PhysRevSTAB.14.032001).
- [7] G. Kazakevich *et al.*, "High-power magnetron transmitter as an RF source for superconducting linear accelerators," *Nucl. Instrum. Methods Phys. Res. A, Accel. Spectrom., Detect. Assoc. Equip.*, vol. 760, pp. 19–27, Oct. 2014, doi: [10.1016/j.nima.2014.05.069](https://doi.org/10.1016/j.nima.2014.05.069).
- [8] T. A. Treado, P. D. Brown, T. A. Hansen, and D. J. Aiguier, "Phase locking of two long-pulse, high-power magnetrons," *IEEE Trans. Plasma Sci.*, vol. 22, no. 5, pp. 616–625, Oct. 1994, doi: [10.1109/27.338275](https://doi.org/10.1109/27.338275).
- [9] Y. Zhang, K. Huang, D. K. Agrawal, T. Slaweck, H. Zhu, and Y. Yang, "Microwave power system based on a combination of two magnetrons," *IEEE Trans. Electron Devices*, vol. 64, no. 10, pp. 4272–4278, Oct. 2017, doi: [10.1109/TED.2017.2737555](https://doi.org/10.1109/TED.2017.2737555).
- [10] C. Liu, H. Huang, Z. Liu, F. Huo, and K. Huang, "Experimental study on microwave power combining based on injection-locked 15-kW S-band continuous-wave magnetrons," *IEEE Trans. Plasma Sci.*, vol. 44, no. 8, pp. 1291–1297, Aug. 2016, doi: [10.1109/TPS.2016.2565564](https://doi.org/10.1109/TPS.2016.2565564).
- [11] Z. Liu *et al.*, "Phase-shifterless power controlled combining based on 20-kW S-band magnetrons with an asymmetric injection," *IEEE Electron Device Lett.*, vol. 39, no. 9, pp. 1425–1428, Sep. 2018, doi: [10.1109/LED.2018.2857808](https://doi.org/10.1109/LED.2018.2857808).
- [12] Z. Liu, X. Chen, M. Yang, P. Wu, K. Huang, and C. Liu, "Experimental studies on a four-way microwave power combining system based on hybrid injection-locked 20-kW S-band magnetrons," *IEEE Trans. Plasma Sci.*, vol. 47, no. 1, pp. 243–250, Jan. 2019, doi: [10.1109/TPS.2018.2876574](https://doi.org/10.1109/TPS.2018.2876574).
- [13] S. Y. Park, Y. R. Heo, J. Y. Kang, D. G. Kim, S. T. Han, and J. J. Choi, "Frequency and phase locking experiments on a 2.45 GHz magnetron," in *Proc. Int. Vac. Electron. Conf. (IVEC)*, Busan, South Korea, Apr. 2019, pp. 1–2.
- [14] C. Lai *et al.*, "Highly efficient microwave power system of magnetrons utilizing frequency-searching injection-locking technique with no phase shifter," *IEEE Trans. Microw. Theory Techn.*, vol. 68, no. 10, pp. 4424–4432, Oct. 2020, doi: [10.1109/TMTT.2020.3006488](https://doi.org/10.1109/TMTT.2020.3006488).
- [15] C. Chen, K. Huang, and Y. Yang, "Microwave transmitting system based on four-way master-slave injection-locked magnetrons and horn arrays with suppressed sidelobes," *IEEE Trans. Microw. Theory Techn.*, vol. 66, no. 5, pp. 2416–2424, May 2018, doi: [10.1109/TMTT.2018.2790924](https://doi.org/10.1109/TMTT.2018.2790924).
- [16] B. Yang, X. Chen, J. Chu, T. Mitani, and N. Shinohara, "A 5.8-GHz phased array system using power-variable phase-controlled magnetrons for wireless power transfer," *IEEE Trans. Microw. Theory Techn.*, vol. 68, no. 11, pp. 4951–4959, Nov. 2020, doi: [10.1109/TMTT.2020.3007187](https://doi.org/10.1109/TMTT.2020.3007187).
- [17] B. Levush, K. L. Jensen, and Y. Y. Lau, "A comparison of flicker noise and shot noise on a hot cathode," *IEEE Trans. Plasma Sci.*, vol. 28, no. 3, pp. 794–797, Jun. 2000, doi: [10.1109/27.887726](https://doi.org/10.1109/27.887726).

- [18] D. Thelen, R. Reynolds, R. Emerson, M. Pearson, A. S. Gilmour, and A. MacMullen, "Characterization of relaxation-oscillation noise in continuous-wave traveling wave tubes," *IEEE Trans. Plasma Sci.*, vol. 32, no. 3, pp. 1057–1065, Jun. 2004, doi: [10.1109/TPS.2004.828810](https://doi.org/10.1109/TPS.2004.828810).
- [19] P. Pengvanich, Y. Y. Lau, J. W. Luginsland, R. M. Gilgenbach, E. Cruz, and E. Schamiloglu, "Effects of frequency chirp on magnetron injection locking," *Phys. Plasmas*, vol. 15, no. 7, Jul. 2008, Art. no. 073110, doi: [10.1063/1.2956332](https://doi.org/10.1063/1.2956332).
- [20] I. M. Rittersdorf, Y. Y. Lau, J. C. Zier, R. M. Gilgenbach, E. J. Cruz, and J. W. Luginsland, "Temporal and spatial locking of nonlinear systems," *Appl. Phys. Lett.*, vol. 97, no. 17, Oct. 2010, Art. no. 171502, doi: [10.1063/1.3506496](https://doi.org/10.1063/1.3506496).
- [21] R. Adler, "A study of locking phenomena in oscillators," *Proc. IEEE*, vol. 61, no. 10, pp. 1380–1385, Oct. 1973, doi: [10.1109/PROC.1973.9292](https://doi.org/10.1109/PROC.1973.9292).
- [22] J. Benford, H. Sze, W. Woo, R. R. Smith, and B. Harteneck, "Phase locking of relativistic magnetrons," *Phys. Rev. Lett.*, vol. 62, no. 8, p. 969, Feb. 1989, doi: [10.1103/PhysRevLett.62.969](https://doi.org/10.1103/PhysRevLett.62.969).
- [23] H.-C. Chang, X. Cao, M. J. Vaughan, U. K. Mishra, and R. A. York, "Phase noise in externally injection-locked oscillator arrays," *IEEE Trans. Microw. Theory Techn.*, vol. 45, no. 11, pp. 2035–2042, Nov. 1997, doi: [10.1109/22.644229](https://doi.org/10.1109/22.644229).
- [24] H.-C. Chang, A. Borgioli, P. Yeh, and R. A. York, "Analysis of oscillators with external feedback loop for improved locking range and noise reduction," *IEEE Trans. Microw. Theory Techn.*, vol. 47, no. 8, pp. 1535–1543, Aug. 1999, doi: [10.1109/22.780406](https://doi.org/10.1109/22.780406).
- [25] R. D. Weglein and H. A. Leach, "The noise behavior of an injection-locked magnetron reflection amplifier," in *IEEE MTT-S Int. Microw. Symp. Dig.*, Palo Alto, CA, USA, Jun. 1987, pp. 261–264, doi: [10.1109/MWSYM.1987.1132379](https://doi.org/10.1109/MWSYM.1987.1132379).
- [26] S. C. Chen, "Growth and frequency pushing effects in relativistic magnetron phase-locking," *IEEE Trans. Plasma Sci.*, vol. 18, no. 3, pp. 570–576, Jun. 1990, doi: [10.1109/27.55928](https://doi.org/10.1109/27.55928).
- [27] K. Li, Y. Zhang, H.-C. Zhu, K.-M. Huang, and Y. Yang, "Theoretical and experimental study on frequency pushing effect of magnetron," *Chin. Phys. B*, vol. 28, no. 11, Oct. 2019, Art. no. 118402, doi: [10.1088/1674-1056/ab4d3d](https://doi.org/10.1088/1674-1056/ab4d3d).



Xiaojie Chen (Graduate Student Member, IEEE) received the B.S. degrees in information counter technology from Southwest University of Science and Technology, Mianyang, China, in 2014, and the M.S. degree in radio physics from Sichuan University, Chengdu, China, in 2018. He is currently pursuing the Ph.D. degree in communication systems and engineering, Sichuan University.

His current research interests include injection locking technology and high-power microwave combining.



Bo Yang (Student Member, IEEE) was born in Taizhou, China, in 1986. He received the B.S. degree in electronic information engineering from the China University of Petroleum, Qingdao, China, in 2008, and the M.E. degree in electronic engineering from Kyoto University, Kyoto, Japan, in 2018, where he is currently pursuing the Ph.D. degree in electronic engineering.

From 2008 to 2015, he was an RF Engineer with the DAIHEN Group, Qingdao.



Naoki Shinohara (Senior Member, IEEE) received the B.E. degree in electronic engineering, and the M.E. and Ph.D. (Eng.) degrees in electrical engineering from Kyoto University, Kyoto, Japan, in 1991, 1993, and 1996, respectively.

Since 1996, he has been with the Radio Science Center for Space and Atmosphere, Kyoto University, Kyoto, Japan. From 2010, he has been a Professor at the Research Institute for Sustainable Humanosphere, Kyoto University. His research interests include solar power station/satellite and microwave power transmission system.

Dr. Shinohara is the IEEE Distinguish Microwave lecturer, IEEE MTT-S Technical Committee 26 (Wireless Power Transfer and Conversion) vice chair, IEEE MTT-S Kansai Chapter TPC member, IEEE Wireless Power Transfer Conference advisory committee member, international journal of Wireless Power Transfer (Cambridge Press) executive editor, Radio Science for URSI Japanese committee C member, past technical committee chair on IEICE Wireless Power Transfer, Japan Society of Electromagnetic Wave Energy Applications vice chair, Wireless Power Transfer Consortium for Practical Applications (WiPoT) chair, and Wireless Power Management Consortium (WPMC) chair.



Changjun Liu (Senior Member, IEEE) received the B.S. degree in applied physics from Hebei University, Baoding, China, in 1994, and the M.S. degree in radio physics and the Ph.D. degree in biomedical engineering from Sichuan University, China, in 1997 and 2000, respectively.

From 2000 to 2001, he was a Post-Doctoral Researcher with Seoul National University, Seoul, South Korea. From 2006 to 2007, he was a Visiting Scholar with Ulm University, Ulm, Germany. Since 1997, he has been with the Department of Radio-Electronics, Sichuan University, where he has been a Professor since 2004. He has authored one book and more than 100 articles. He holds more than 10 patents. His current research interests include microwave power combining of large-power vacuum components, microwave wireless power transmission (WPT), and microwave power industrial applications.

Dr. Liu was a recipient of several honors such as the outstanding reviewer for the IEEE TRANSACTIONS ON MICROWAVE THEORY AND TECHNIQUES from 2006 to 2010, support from the MOE under the Program for New Century Excellent Talents in University, China, from 2012 to 2014, the Sichuan Province Outstanding Youth Fund from 2009 to 2012, and named by Sichuan Province as an Expert with Outstanding Contribution. He is the Associate Editor of the *Chinese Journal of Applied Science*.